The sine-Gordon Equation and its Application to Black Holes

by

Mohammed O. S. Al Humaidi

Bachelor of Science in Mathematics, Taif University, 2003

A REPORT SUBMITTED IN PARTIAL FULFILLMENT OF THE REQUIREMENTS FOR THE DEGREE OF

MASTER OF SCIENCE

In the Graduate Academic Unit of Mathematics and Statistics

Supervisor:	Sanjeev. Seahra, Ph.D., Dept. of Mathematics and Statistics
Examining Board:	Viqar. Husain, Ph.D., Dept. of Mathematics and Statistics
	Lin. Wang, Ph.D., Dept. of Mathematics and Statistics

This report is accepted

Dean of Graduate Studies

THE UNIVERSITY OF NEW BRUNSWICK

January, 2015

Abstract

Linear and nonlinear wave equations are important in various aspects of mathematics and physics, including the study of black holes. After a brief survey of the sine-Gordon equation (SGE), this report presents a fourth-order numerical approximation scheme for solving equations of this type. This is followed by a numerical investigation of SGE in the presence of the Pöschl-Teller potential. We close with a discussion of the application of this method to the study of black hole dynamics.

Dedication

This work is dedicated to my beloved parents, who inspired me and sparked my interest in pursuing higher education, who praying for me and who provided me with support, help and encouragement every moment along the long academic road that I have followed. To my wife, who has been a constant source of support and encouragement during the challenges of graduate school and life. I am truly thankful for having you in my life. To my two daughters, who have always loved me. To all those special and precious people in my life, I could not have completed this effort without their assistance and enthusiasm. Thank you all. I am very fortunate to have you in my life.

Acknowledgements

I would like to convey my sincere thanks to my research supervisor: Prof. Sanjeev Seahra for all of his help with my studies at the University of New Brunswick particularly in the writing of this thesis, and for his advice on issues both within and without the scope of my studies. His guidance and encouragement have been invaluable to me. I also wish to thank Prof. Viqar Husain as well as Prof. Lin Wang, for their careful review of my thesis and for suggesting many improvements. I would like to thanks the faculty and staff of the Department of Mathematics and Statistics for their assistance with all aspects of my studies at the University of New Brunswick.

This work was supported by the Ministry of Higher Education in Saudi Arabia.

Table of Contents

List of Figures

Chapter 1

Introduction

In this chapter, we introduce the sine-Gordan equation and some of its modifications and demonstrate how it arises when one studies the dynamics of mechanical transmission lines.

1.1 The sine-Gordan equation and its modifications

The sine-Gordon equation (SGE) is a nonlinear hyperbolic partial differential equation of the form

$$\psi_{tt} - \psi_{xx} + \sin\psi = 0, \tag{1.1}$$

where $\psi = \psi(x,t)$. This equation has many solutions, some of which are soliton solutions. A soliton is self-reinforcing solitary wave, or pulse, which

maintains its velocity and shape. This equation first arose in the study of surfaces of constant negative curvature [1]. The equation also appears in a number of physical applications including relativistic field theory [1], Josephson junctions [1] and mechanical transmission lines [9].

Modified sine-Gordan equations (MSGEs) also appear in applications. An example is that of the long Josephson junction, which is governed by

$$\psi_{tt} - \psi_{xx} + \sin\psi = -\alpha\psi_t + \gamma, \tag{1.2}$$

where α is the dimensionless damping parameter, and γ is a normalized bias current. Another example occurs when considering a field ψ propagating around a black hole with a self-interaction $\propto \sin\psi$ [3]. The equation of motion for such a field is

$$\psi_{tt} - \psi_{xx} + V(x)\psi + Q(x)\sin\left(\frac{\psi}{\rho(x)}\right) = 0. \tag{1.3}$$

where $V(x)$ is the "spatially dependent" potential appearing in the study of quasinormal modes of scalar field about black holes [8], while $\rho(x)$ and $Q(x)$ are known functions.

In this report we will discuss the analytic and numeric solution of the SGE and certain MSGEs. Our purpose in studying SGE in chapter 2 is to establish some of its fundamental properties, including the presence of soliton solutions and the use of the Bäcklund transformation to generate these solutions. We will then develop a numerical scheme for the investigation of

MGSE in Section 3. Our results from Section 2 will be used as a test for the numerical scheme and as a basis for comparison with MSGE. In particular, we will investigate how the introduction of the Pöschl-Teller potential affects the behaviour of the evolution of the moving breather solution to SGE.

1.2 Application: mechanical transmission lines

Before discussing the solution of the SGE in the next chapter, we present a detailed derivation of how the equation arises from an analysis of the dynamical of a mechanical transmission line, following the treatment in [9].

A mechanical transmission line consists of a series of pendula connected by a steel spring and supported horizontally by a thin wire, as shown in Figure 1.1. Each pendulum is free to swing in a plane perpendicular to the wire. A displacement in any pendulum results in a force that causes a wave to propagate through the line. A dramatic effect occurs if a single pendulum at one end is quickly turned one full revolution around the wire. This causes the formation of a kink, as shown in Figure 1.2.

We assume that each pendulum has mass m and length l, and that neighbors are a fixed distance Δx apart. We use $\psi_i(t)$ to denote the angle of rotation of the i^{th} pendulum from its equilibrium position at time t, as shown in Figure 1.3. The gravitational force $-mg$ acting on the i^{th} pendulum produces a tangential force $mg\sin(\psi_i)$ which tries to rotate the pendulum

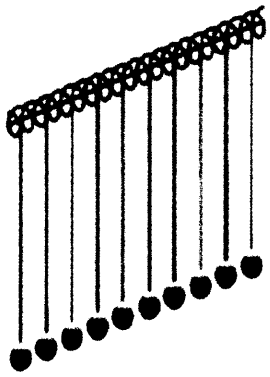

Figure 1.1: Pendula attached to horizontal spring. [R. Knoble, 2000]

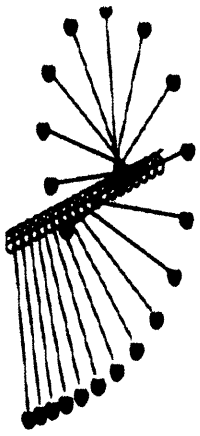

Figure 1.2: A large disturbance moving down the pendulum line. [R. Knoble, 2000]

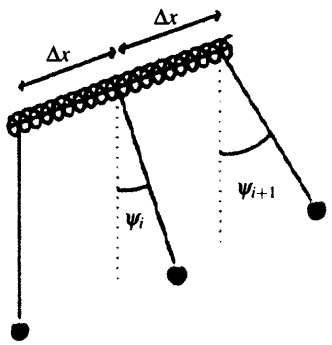

Figure 1.3: Angles of rotation of the pendula. [R. Knoble, 2000]

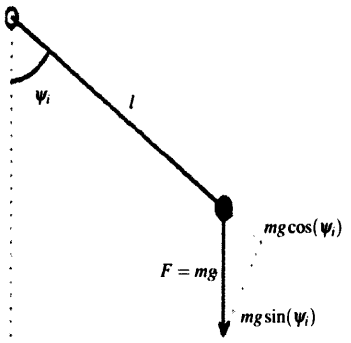

Figure 1.4: The gravitational force acting on the i^{th} pendulum. [R. Knoble, 2000]

downward, as shown in Figure 1.4. The force equation for planar pendulum is given by

$$F = -mgl \sin \psi \tag{1.4}$$

where g is the gravity constant. By Hooke's, law the torque on node i from the spring is given by

$$S_{i-1,i} + S_{i,i+1} = k \frac{\psi_{i+1} - 2\psi_i + \psi_{i-1}}{\Delta x}, \tag{1.5}$$

where k is the spring constant. Adding the force of gravity to (1.5), and setting l, g, and k to be equal to 1 yields

$$m \frac{d^2 \psi_i}{dt^2} = \frac{\psi_{i+1} - 2\psi_i + \psi_{i-1}}{\Delta x} - m \sin \psi_i \tag{1.6}$$

Now divide (1.6) by Δx and take the limit $\Delta x \to 0$. Suppose that m changes with Δx so that $m/\Delta x = 1$. In the limit, we obtain:

$$\psi_{tt} - \psi_{xx} + \sin \psi = 0,$$

which is the SGE.

Chapter 2

The sine-Gordon Equation

In this chapter, we discuss some of the analytic properties of SGE. We begin with a derivation of the form of SGE in characteristic coordinates. This is followed by a discussion of Bäcklund's transformation and its usefulness in generating new solutions from known ones. We then discuss the kink-antikink, standing breather, and moving breather solutions.

2.1 Characteristic coordinates

Much of the analysis of the SGE is easier if one transforms to characteristics coordinates (u, v), defined by

$$u = t - x, \qquad v = t + x. \tag{2.1}$$

We now show that SGE in these coordinates takes the form

$$4\psi_{uv} = -\sin\psi \tag{2.2}$$

where $\psi = \psi(u, v)$. Computing partial derivatives with respect to t and x, and using $\psi_{uv} = \psi_{vu}$, we find

$$\psi_{tt} = \psi_{ut}\psi_{vt} = \psi_{uu} + 2\psi_{uv} + \psi_{vv}, \tag{2.3}$$

$$\psi_{xx} = -\psi_{ux} + \psi_{vx} = \psi_{uu} - 2\psi_{uv} + \psi_{vv}. \tag{2.4}$$

Subtracting (2.3) from (2.4) gives us

$$\psi_{tt} - \psi_{xx} = 4\psi_{uv}. \tag{2.5}$$

Finally, substituting (2.5) into (1.1) gives us SGE in characteristic coordinates

$$4\psi_{uv} = -\sin\psi.$$

2.2 Bäcklund's transformation

2.2.1 The basic idea

Bäcklund transformation for SGE is the first-order system of partial differential equation given by

$$\psi_u + \eta_u = \lambda \sin\left(-\frac{1}{2}\psi + \frac{1}{2}\eta\right), \quad \psi_v - \eta_v = \frac{1}{\lambda}\sin\left(\frac{1}{2}\psi + \frac{1}{2}\eta\right), \tag{2.6}$$

where ψ=$\psi(u,v)$, η=$\eta(u,v)$, and $\lambda \neq 0$ is an arbitrary parameter. From a known solution of SGE, it is possible to generate a new solution through the Bäcklund transformation. This is done by starting with a known solution η of SGE and solving for ψ in (2.6). Then ψ must be a new solution of SGE.

Theorem 2.2.1. *Let ψ and η be solutions to (2.6). Then ψ and η both satisfy SGE.*

Proof. Differentiating the first equation in (2.6) with respect to v, we obtain

$$\psi_{uv} + \eta_{uv} = -\frac{1}{2}\lambda \cos\left(-\frac{1}{2}\psi + \frac{1}{2}\eta\right)\,(\psi_v - \eta_v)\,. \tag{2.7}$$

Now substitute the term $\psi_v - \eta_v$ with its value in (2.6) to obtain

$$\psi_{vu} + \eta_{vu} = -\frac{1}{2}\cos\left(-\frac{1}{2}\psi + \frac{1}{2}\eta\right)\sin\left(\frac{1}{2}\psi + \frac{1}{2}\eta\right). \tag{2.8}$$

Differentiating the second equation in (2.6) with respect to u gives us

$$\psi_{vu} - \eta_{vu} = \frac{1}{2\lambda} \cos\left(\frac{1}{2}\psi + \frac{1}{2}\eta\right)(\psi_u + \eta_u). \tag{2.9}$$

Now substitute the term $\psi_u + \eta_u$ with its value in (2.6) to obtain

$$\psi_{vu} - \eta_{vu} = \frac{1}{2} \cos\left(\frac{1}{2}\psi + \frac{1}{2}\eta\right) \sin\left(-\frac{1}{2}\psi + \frac{1}{2}\eta\right). \tag{2.10}$$

By adding (2.10) and (2.8), and using the addition law for sine, together with $\eta_{uv} = \eta_{vu}$ and $\psi_{uv} = \psi_{vu}$, we obtain

$$2\psi_{uv} = -\cos\left(\frac{1}{2}\psi\right) \sin\left(\frac{1}{2}\psi\right). \tag{2.11}$$

Now using the double angle formula for sine, we obtain

$$2\psi_{uv} = -\frac{1}{2}\sin(\psi). \tag{2.12}$$

Multiplying the last equation by 2, we finally arrive at

$$4\psi_{uv} = -\sin(\psi). \tag{2.13}$$

In similar fashion, subtracting (2.10) from (2.8) yields

$$2\eta_{uv} = -\frac{1}{2}\sin(\eta). \tag{2.14}$$

Multiplying the last equation by 2 then gives us

$$4\eta_{uv} = -\sin(\eta). \tag{2.15}$$

Equations (2.13) and (2.15) show that ψ and η are both solutions to SGE as claimed. □

2.2.2 Kink-antikink solutions

The Bäcklund transformation for SGE is given by (2.6). If η is a solution of SGE, and ψ and η satisfy Bäcklund Transformation, then ψ is also a solution of SGE. We now show how this can be used to generate new solutions from known ones.

Let's start with the trivial solution $\eta(u, v) = 0$. Then, on temporarily setting $\bar{u} = \lambda u$, $\bar{v} = v/\lambda$, the pair of equations in (2.6) reduce to

$$\psi_{\bar{u}} = \sin\left(-\frac{\psi}{2}\right), \quad \psi_{\bar{v}} = \sin\left(\frac{\psi}{2}\right). \tag{2.16}$$

Adding these equations yields

$$\psi_{\bar{u}} + \psi_{\bar{v}} = 0, \tag{2.17}$$

which has the general solution

$$\psi = f(\bar{u} - \bar{v}) \equiv f(y), \tag{2.18}$$

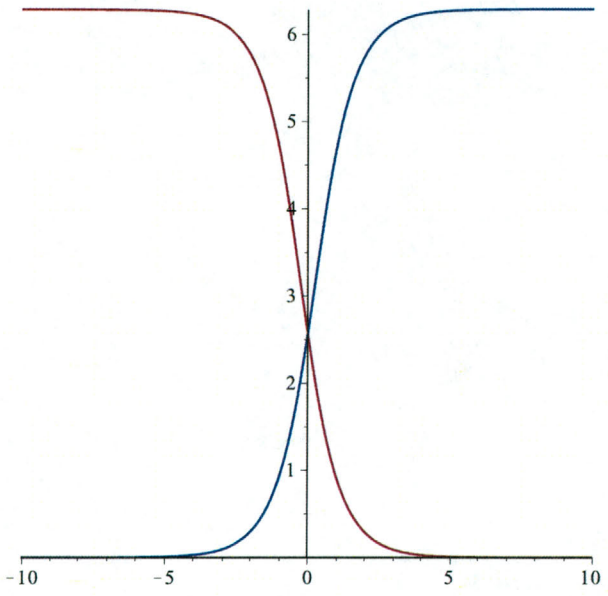

Figure 2.1: Representation of the kink (blue) and antikink (red) solutions.

where $y = \bar{u} - \bar{v}$.

Now $\psi_{\bar{u}} = (df/dy)(dy/d\bar{u}) = (df/dy)$ and $\psi_{\bar{v}} = -df/dy$, so that, on subtracting the second equation in (2.16) from the first equation, we obtain

$$2\frac{df}{dy} = -2\sin\left(\frac{f}{2}\right). \tag{2.19}$$

Integrating (2.19) yields

$$\ln\tan\left(\frac{f}{4}\right) = y + \text{constant}. \tag{2.20}$$

Solving for f and changing back to our original variables gives us

$$\psi(u,v) = 4\arctan\left(A\exp\left(\lambda(u - v/\lambda^2)\right)\right). \tag{2.21}$$

Equation (2.21) gives the kink-anitkink solutions of SGE in characteristic coordinates, where $A = e^{-x_0/\sqrt{1-c^2}}$ and $\lambda = \pm\frac{1}{2}\sqrt{(1-c)/(1+c)}$. We substitute (2.1) into (2.21). The solution of SGE take the form[1]

$$\psi(x,t) = 4\arctan\left(\exp\left(\pm\frac{x - x_0 - ct}{\sqrt{1-c^2}}\right)\right). \tag{2.22}$$

This represents a localized solitary wave, travelling at a constant speed $|c| < 1$. The $\pm$ signs correspond to the kink and antikink solutions, respectively, which are plotted in figure 2.1.

2.2.3 Breather solutions

The sine-Gordon equation also has a family of soliton solutions known as the standing breather. A breather is a nonlinear mode that is localized in space and oscillates with time. These can be generated by applying the Bäcklund transformation to the kink-antiknk solutions. The resulting solution has the form [3]

$$\psi(x,t) = 4\arctan\left(\frac{2\sin(t/\sqrt{5})}{\cosh(2x/\sqrt{5})}\right). \tag{2.23}$$

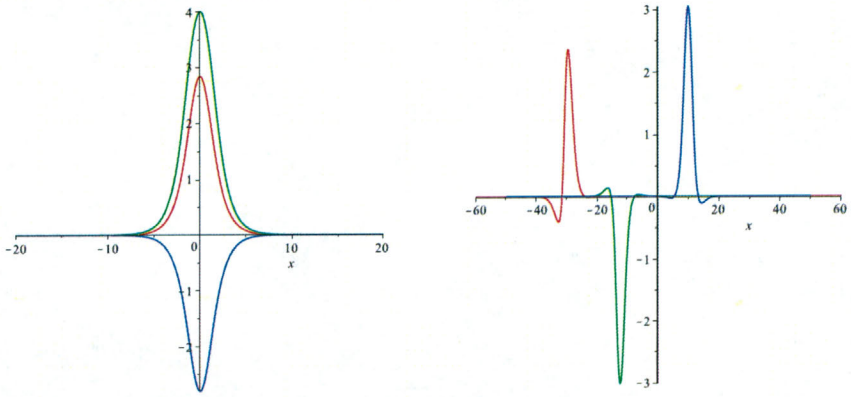

(a) (b)

Figure 2.2: The Breather solution, (a) Stander Breather, calculated for three different times $t = 1$ (red curve), $t = 2$ (green curve), $t = 8$ (blue curve, and (b) The moving Breather, calculated for three different times $t = -60$ (red curve), $t = -25$ (green curve), $t = 20$ (blue curve), where $c = 0.5$ and $\mu = \pi/4$.

The moving breather solution has the form [4]

$$\psi(x,t) = 4\arctan\left(\tan\mu\frac{\cos(\gamma\cos\mu(t-xc))}{\cosh(\gamma\sin\mu(x-ct))}\right), \tag{2.24}$$

where $\gamma = 1/\sqrt{1-c^2}$, μ is a parameter that determines the size and frequency of the pulse and c is the speed of the pulse. We will use this solution as initial data for simulations in Chapter 3.

Chapter 3

The Modified sine-Gordon Equation

We are interested in studying numerical solutions of a MSGE that is similar to SGE

$$\psi_{tt} - \psi_{xx} = F(\psi). \tag{3.1}$$

We are particularly interested in the case

$$F(\psi) = -V\psi - \sin\psi, \tag{3.2}$$

where $\psi = \psi(x,t)$, and $V = V(x)$ is a potential independent of time. This class of MSGEs is similar to the equations of motion of self-interacting scalar fields about black holes. We note that there are no known analytic solution to the MSGE. In this chapter we explore a numerical method for solving the

MSGE.

3.1 The modified sine-Gordon equation and its discretization

We now describe a method to discretize MSGE in characteristic coordinates (u, v). In characteristic coordinates MSGE has the form

$$\psi_{uv} = \frac{1}{4}F(\psi). \tag{3.3}$$

We use ψ_S, ψ_E, ψ_W, and ψ_N to denote $\psi_S = \psi(u_i, v_j)$, $\psi_W = \psi(u_i + h, v_j)$, $\psi_E = \psi(u_i, v_j + h)$ $\psi_N = \psi(u_i + h, v_j + h)$, respectively. Here, h is the step size.

Our goal is to find a discrete method that allows us to compute ψ_N from ψ_S, ψ_E, and ψ_W. Given the stencil, we find a discrete (approximate) solution as follows. Choose initial conditions along the lower diagonal edges (u, v) in Figure 3.1(a), and then use the stencil to generate an approximation to ψ in the whole domain.

3.1.1 Derivation of the stencil

We first derive an integral form of MSGE. Let the centre of a cell Q in computational grid have coordinates $M(u_0, v_0)$. Then $\psi_S = \psi(u - \frac{h}{2}, v - \frac{h}{2})$, $\psi_W = \psi(u - \frac{h}{2}, v + \frac{h}{2})$, $\psi_E = \psi(u + \frac{h}{2}, v - \frac{h}{2})$ and $\psi_N = \psi(u + \frac{h}{2}, v + \frac{h}{2})$, where

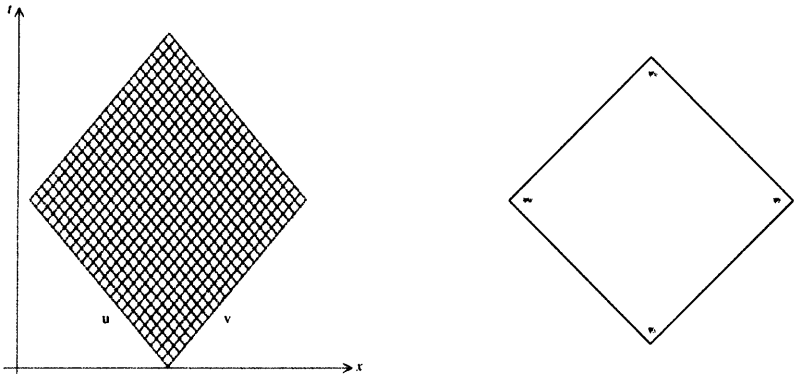

(a) (b)

Figure 3.1: (a) Computation grid in the domain D, and (b) Dcell.

h is the step size. Now integrate (3.3) over the cell Q to obtain

$$\iint_Q \psi_{uv} du dv = \frac{1}{4} \iint_Q F(\psi) du dv. \tag{3.4}$$

By Fubini's theorem, the left-hand side of (3.4) is

$$\iint_Q \psi_{uv} du dv = \int_{-\frac{h}{2}}^{\frac{h}{2}} \left(\int_{-\frac{h}{2}}^{\frac{h}{2}} \psi_{uv}(u+s, v+t) dt \right) ds. \tag{3.5}$$

Evaluating the right hand side of (3.5), we get

$$\int_{-\frac{h}{2}}^{\frac{h}{2}} \left(\int_{-\frac{h}{2}}^{\frac{h}{2}} \psi_{uv}(u+s, v+t) dt \right) ds = \psi_N - \psi_E - \psi_W + \psi_S. \tag{3.6}$$

Thus (3.6) can be rewritten as

$$\psi_N - \psi_E - \psi_W + \psi_S = \frac{1}{4}\iint_Q F(\psi)dudv. \tag{3.7}$$

Equation (3.7) is the integral form of (3.3). To approximate the right-hand side of (3.7), let's define $G(u,v) = F(\psi(u,v))$. We write $G^M = G(u,v)$ for the value of G at the centre of Q. Similarly, we define $G_u^M = \left(\frac{\partial G}{\partial u}\right)|_{(u_0,v_0)}$ and $G_v^M = \left(\frac{\partial G}{\partial v}\right)|_{(u_0,v_0)}$. Then the Taylor series expansion for G about M to first order is

$$G(u+s, v+t) = G^M + sG_u^M + tG_v^M + O(h^2). \tag{3.8}$$

Plugging $s = h/2$, $t = -h/2$ into (3.8) then yields

$$G^E = G^M + \frac{h}{2}G_u^M - \frac{h}{2}G_v^M + O(h^2). \tag{3.9}$$

On the other hand, plugging $s = -h/2$, $t = h/2$ into (3.8) gives

$$G^W = G^M - \frac{h}{2}G_u^M + \frac{h}{2}G_v^M + O(h^2). \tag{3.10}$$

The average of (3.9) and (3.10) is then seen to be

$$\frac{1}{2}(G^E + G^W) = G^M + O(h^2). \tag{3.11}$$

Hence

$$\iint_Q G(s,t)ds\,dt = \iint_Q \left(G^M + sG_u^M + tG_v^M + O(h^2)\right) ds\,dt. \tag{3.12}$$

Since G^M, G_u^M and G_v^M are constant, we have

$$\iint_Q G(s,t)ds\,dt = G^M \iint_Q dsdt + G_u^M \iint_Q sdsdt + G_v^M \iint_Q tds\,dt + O(h^2) \iint_Q ds\,dt. \tag{3.13}$$

We now observe that

$$\iint_Q ds\,dt = h^2, \text{ and } \iint_Q sds\,dt = \iint_Q tds\,dt = 0, \tag{3.14}$$

so

$$\iint_Q G(s,t)dsdt = G^M h^2 + O(h^4). \tag{3.15}$$

Substituting (3.11) into (3.15), we get

$$\iint_Q G(s,t)ds\,dt = \left(\frac{1}{2}(G^E + G^W) + O(h^2)\right) h^2 + O(h^4), \tag{3.16}$$

which simplifies to

$$\iint_Q G(s,t)dsdt = \frac{h^2}{2}(G^E + G^W) + O(h^4). \tag{3.17}$$

Noting that $G^E = F(\psi_E)$ and $G^W = F(\psi_W)$, this becomes

$$\iint_Q F(\psi)dudv = \frac{h^2}{2}\left(F(\psi_E) + F(\psi_W)\right) + O(h^4). \tag{3.18}$$

Finally substituting (3.18) into the right-hand side of (3.7) yields

$$\psi_N = \psi_E + \psi_W - \psi_S + \frac{h^2}{8}\left(F(\psi_E) + F(\psi_W)\right) + O(h^4). \tag{3.19}$$

This is the stencil we will use for simulations. Note that the one-step error is $O(h^4)$.

3.2 Comparing numerical and analytic results for the SGE

We now use the method developed in the previous section to obtain a numerical approximation to a known solution of the SGE. We then compare the numerical approximation to the known solution by computing the root mean square error (RMSE) of their difference. This allows us to see how well the approximation method works. There are two types of error are important to identify: local error and global error. In practice, we are only concerned with the global (cumulative) error. The global discretization error is given

by (RMSE) $\mathcal{E}$ of $\psi^{\text{num}} - \psi^{\text{exact}}$, which is defined to be

$$\mathcal{E} = \left(h^2 \sum_{\Omega} (\psi^{\text{num}} - \psi^{\text{exact}})^2 \right)^{1/2} \tag{3.20}$$

where the sum is taken over all cells Ω, ψ^{num} is the numerical solution and ψ^{exact} is the exact solution, evaluated on the competition grid. We now verify empirically that $\mathcal{E} = O(h^2)$ for $F(\psi) = -\sin(\psi)$, we then explain why this is the case.

We construct a numerical approximation of the moving breather as follows:

1. Start with initial conditions for the exact solution of moving breather of SGE in (x, t) coordinates.

2. Convert the initial conditions to characteristic coordinates (u, v).

3. Solve for $\psi(u, v)$ numerically using the stencil with $F(\psi) = -\sin(\psi)$.

4. The analytic solution is known in this case, so we can explicitly calculate the global error $\mathcal{E}$ between the numerical solution and the exact solution.

Figure 3.2 is a log-log plot of the computed RMSE for various choices of the step size h. We fix the length of the sides of the computation grid to be L so that $h = L/N$, where N is the number of steps in each direction. The slope of this plot is approximately -2, indicating that the global error is $O(h^2)$. We expect the global error $\mathcal{E}$ to obey

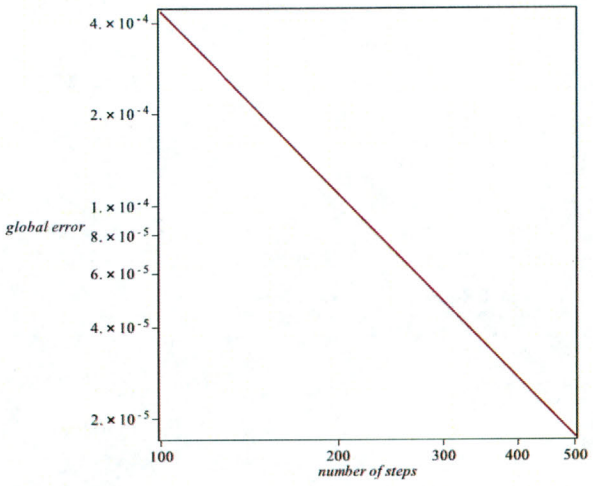

Figure 3.2: Log-log plot of global error $\mathcal{E}$ as a function of N.

$$\begin{aligned}\mathcal{E} &\simeq \text{(number of steps)} \times \text{(one-step error for each step)} \\ &= N^2 \times O(h^4) \\ &= O\left(\frac{1}{h^2}\right) \times O(h^4) = O(h^2).\end{aligned} \tag{3.21}$$

This agrees with our empirical result.

3.3 Numerical investigations of the MSGE

Now we construct a numerical approximation of the modified sine-Gordon Equation. First, let us define the inverted Pöschl-Teller potential by $V(x) = \text{sech}(\beta x)$ where β is a parameter. The potential barrier $V(x)$ has exponential decay with a "small footprint" for large β and a "large footprint" for small β, as shown in Figure 3.3.

We carry out our experiments as follows:

1. Start with initial conditions for the exact solution of the moving breather of SGE in (x, t) coordinates.

2. Convert the initial conditions to characteristic coordinates (u, v).

3. Solve numerically using the stencil (3.19) with $F(\psi) = -V\psi - \sin\psi$.

We set the initial position at $x_0 \ll 0$, so that the initial wave form is far away from $V(x)$, which is centred at 0. Observe that, for fixed t, $\psi(x, t)$ essentially compact support, so it does not see the potential barrier $V(x)$ for small values of t. Thus, the waveform $\psi(x, t)$ starts to evolve according SGE.

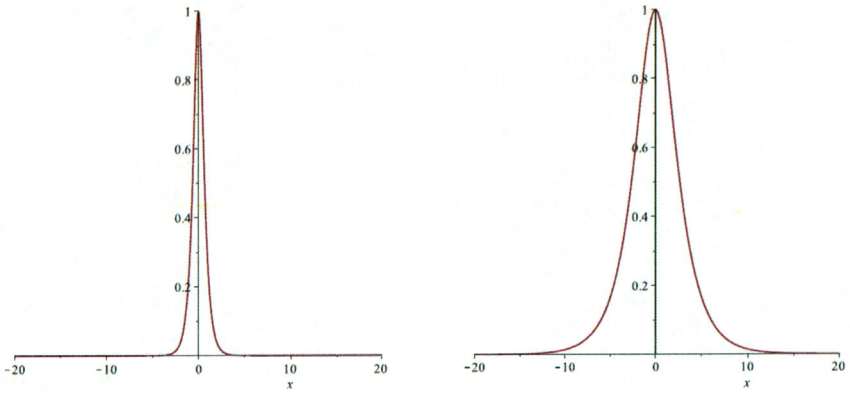

(a) (b)

Figure 3.3: The potential barrier $V(x)$ plots, (a) for large $\beta = 5$, and (b) small values of $\beta = 0.5$.

The resulting evolution of the initial wave form for $\beta = 5$ and $x_0 = -50$ is shown for various values of t in Figure 3.4. We see that ψ begins to move as it does in SGE in (a). In (b) and (c) it interacts with the potential $V(x)$. Then in (d), we see that ψ has split into two waves of roughly equal size moving opposite directions. It appears that half the wave has been reflected by the potential $V(x)$ and the other half has been transmitted. The linear and log-linear plot of the reflected wave as a function of v is shown in Figure 3.5.

When we decrease β to $\beta = 0.5$, making $V(x)$ wider, we see similar behaviour in Figure 3.6, except that most of the wave is reflected this time. The linear and log-linear plot of the reflected wave as a function of v is

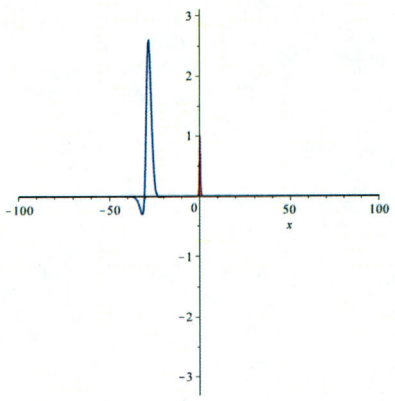

$t = 10$
(a)

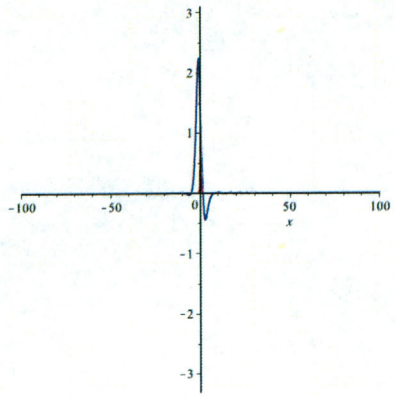

$t = 26$
(b)

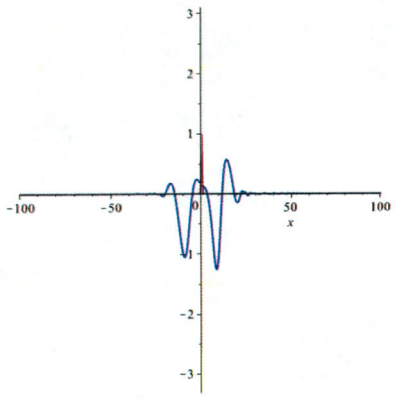

$t = 37$
(c)

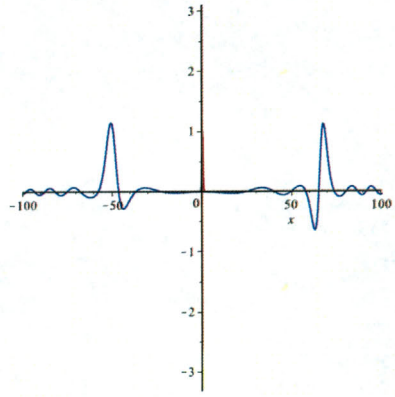

$t = 48$
(d)

Figure 3.4: Evolution of initial wave form for $\beta = 5$ and $x_0 = -50$ at various times t.

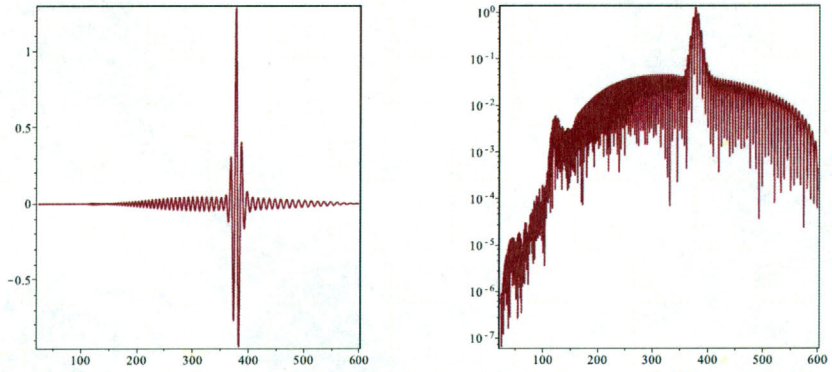

(a) (b)

Figure 3.5: For $\beta = 5$ and $x_0 = -50$: (a) plot reflected wave, and (b) log-linear plot of the reflected wave.

shown in Figure 3.7. This shows a pattern of late time exponential damping in the waveform in the case of the wide potential (with $\beta = 0.5$). Damping of the waveform is present in the case of the narrow potential ($\beta = 5$) as well, but it does not appear to be exponential. The reflected wave forms for both the broad and narrow potentials seem to show the presence of multiple frequencies. They also show a distinct "forward pulse" before the main part of the wave. This forward pulse is more pronounced for the wide potential.

3.4 The rate of convergence of a numerical solutions to the true solution

In absence of the true solution it is still possible to test the rate of convergence of numerical solutions to the true solution. This is done by using the stencil (3.19) twice: once with a stepsize $2h$ and once with stepsize h. The numeric solution generated when the stepsize is $2h$ will be denoted by $\psi_{i,j}^{(2h)} = \psi(u,v) + O(h^2)$. Similarly, when the stepsize is h the numeric solution is labelled as $\psi_{2i,2j}^{(h)} = \psi(u,v) + O(h^2)$, where $u = u_0 + 2ih$, $v = v_0 + 2jh$, and $i, j = 0, 1, ...N/2$. The norm between the numerical solutions with stepsize h and $2h$ given by

$$\widehat{\mathcal{E}} = \left(\frac{1}{(\frac{N}{2}+1)^2} \sum_{i,j=0}^{N/2} (\psi_{i,j}^{(2h)} - \psi_{2i,2j}^{(h)})^2 \right)^{1/2} \tag{3.22}$$

where $N/2$ is the number of steps in each direction.

We now show that $\widehat{\mathcal{E}}$ is of order $O(h^2)$. First, note that by actual error

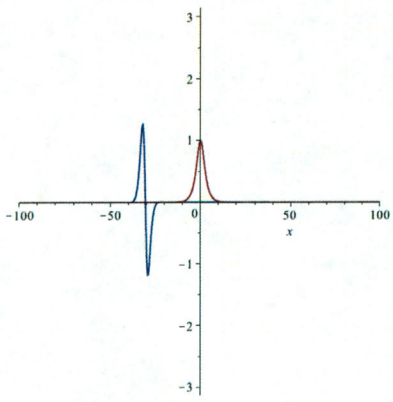

$t = 10$
(a)

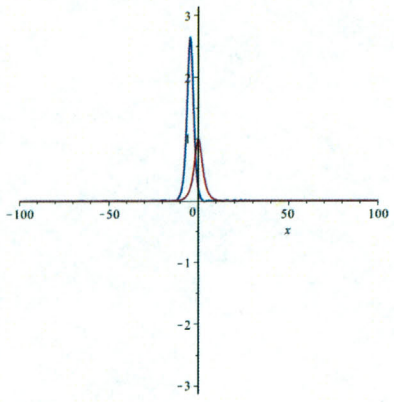

$t = 26$
(b)

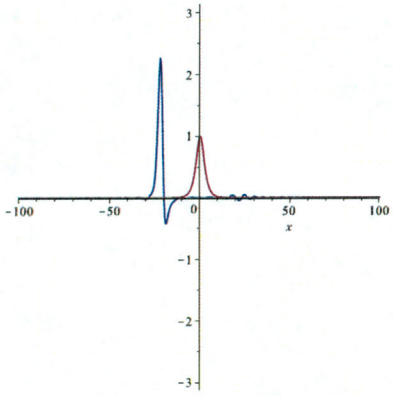

$t = 37$
(c)

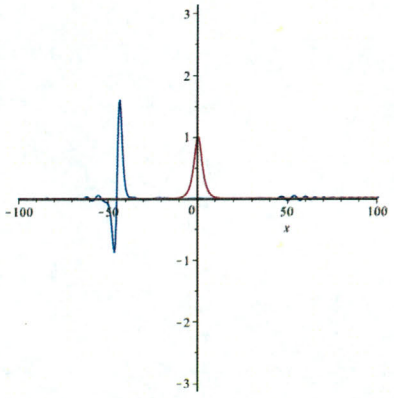

$t = 48$
(d)

Figure 3.6: Evolution of initial wave form for $\beta = 0.5$ and $x_0 = -50$ at various times t

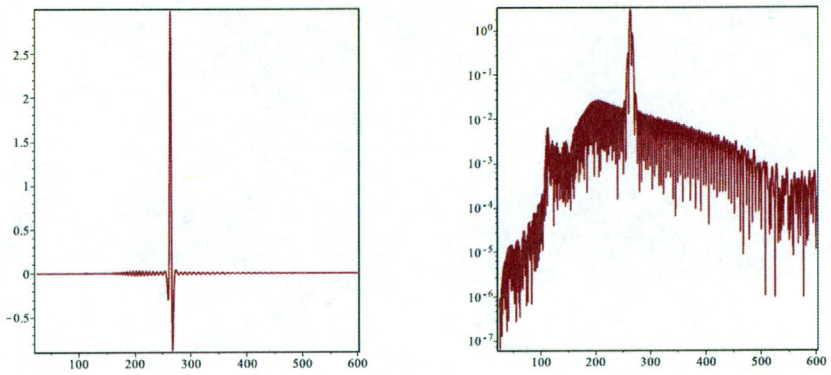

(a) (b)

Figure 3.7: For $\beta = 0.5$ and $x_0 = -50$: (a) plot of the reflected wave, and (b) log-linear plot of the reflected wave.

on the computation grid

$$\psi(u, v) = \psi_{i,j}^{(2h)} + (N/2)^2 O(h^4), \tag{3.23}$$

but $(N/2)^2 = O(h^{-2})$, hence $O(h^{-2})O(h^4) = O(h^2)$, which yields

$$\psi(u, v) = \psi_{i,j}^{(2h)} + O(h^2). \tag{3.24}$$

Similarly

$$\psi(u, v) = \psi_{2i,2j}^{(h)} + O(h^2), \tag{3.25}$$

where $\psi(u,v)$ is the exact solution. Now subtract (3.25) from (3.24) to obtain

$$\psi_{i,j}^{(2h)} - \psi_{2i,2j}^{(h)} = O(h^2), \tag{3.26}$$

noting that

$$(\psi_{i,j}^{(2h)} - \psi_{2i,2j}^{(h^2)})^2 = O(h^4). \tag{3.27}$$

Therefore

$$\sum_{i,j=0}^{N/2} (\psi_{i,j}^{(2h)} - \psi_{2i,2j}^{(h)})^2 = O(h^{-2})O(h^4) = O(h^2), \tag{3.28}$$

we finally arrive at

$$\left(\frac{1}{(\frac{N}{2}+1)^2} \sum_{i,j=0}^{N/2} (\psi_{i,j}^{(2h)} - \psi_{2i,2j}^{(h)})^2 \right)^{1/2} = \left(O(h^2)O(h^2)\right)^{1/2} = O(h^2). \tag{3.29}$$

Equation(3.29) shows that the rate of convergence statistic of $\widehat{\mathcal{E}}$ is of order $O(h^2)$. Figure 3.8 is a log-log plot of the rate of convergence for various choices of the step size h. We fix the length of the sides of the computation grid to be L so that $h = L/N$. The slope of this plot is approximately 2, indicating that the rate of convergence is of order $O(h^2)$.

3.5 Summary

In this chapter, we derived an $O(h^4)$ numerical approximation scheme in Section 3.1 that applies to a class of equations similar to SGE. We then

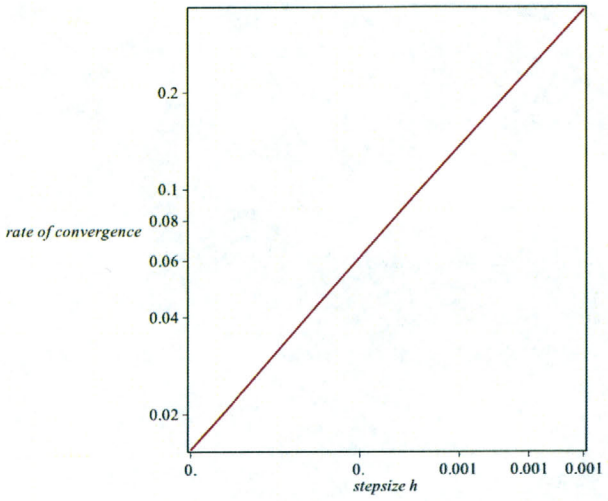

Figure 3.8: For $\beta = 5$: Log-log plot of the rate of convergence for various choices of the step size h.

compared a known solution to its numerical approximation in Section 3.2 to empirically test the accuracy of the method. In section 3.3, we engaged in a numerical study of the behavior of a localized traveling wave (the moving breather) as it passed through the inverted Pöschl-Teller potential. We found that the potential barrier caused part of the wave to be reflected while the rest was transmitted through the barrier. Log-linear plots showed a pattern of exponential damping in the wave form in the case of the wide potential (with $\beta = 0.5$), and non-exponential damping for the narrow potential ($\beta = 5$). It would be interesting to develop an analytic understanding of these late time wave tails. Finally, in section 3.4 we showed the the rate of convergence of the method is $O(h^2)$.

Chapter 4

Conclusions

After reviewing essential aspects of the sine-Gordon equation and its applications to physics, we introduced a modified form of the equation that is relevant to the study of black holes.

We then derived an $O(h^4)$ numerical method for approximating the solutions of the modified sine-Gordan equation and showed that it leads to an $O(h^2)$ global error. Empirical evidence of these accuracy claims was obtained by comparing an exact solution to the sine-Gordon equation with its numerical approximation.

We then we used the method to investigate the effect of adding a potential term to SGE. We found that part of a traveling wave form was transmitted through the potential barrier and part of it was reflected. The amount that was reflected depended on the shape of the potential. We then verified the method converge with a rate $O(h^2)$.

In conclusion, we have introduced a numerical method for solving nonlinear wave equations of a certain type. Its use in the numerical investigation of solutions to such equations as the modified sine-Gordon equation should provide new insight into black hole dynamics.

Bibliography

[1] David Jaderberg, *Fourth order accurate numerical solution of the Sine-Gordon equation*, Uppsala University, 2013

[2] Bernard Piett and W. J. Zakrzewski, *Scattering of Sine-Gordon Kinks on potential wells*, University of Durham, 2013

[3] Sanjeev S. Seahra, *Project on nonlinear wave equation*, University of New Brunswick, 2012

[4] Paul Rigge, *Numerical Solutions to the sine-Gordon Equation*, University of Michigan, 2012

[5] Bernard Piette and W.J. Zakrzewski, *Scattering of Sine-Gordon kinks on potential wells*, University of Durham, 2006

[6] Sanjeev S. Seahra, *An Introduction to black holes*, University of New Brunswick, 2006

[7] Robert M. Wald, *General Relativity*, 1983

[8] Hans-Peter Nollert, *The characteristic sound of black holes and neutron stars*, 1999

[9] Roger Knoble, *An Introduction to the Mathematical Theory of Wave*, 2000

[10] Richard H. Enns and George C. McGuire, *Nonlinear physics with Mathematica for Scientists and Engineers*, 2001

[11] *En.wikipedia.org/wiki/Long_Josephson_junction*

[12] Carlos O. Lousto and Richard H. Price, *Understanding initial data for black hole collisions*, 1997

Vita

Candidate's full name:

Mohammed Othman Al Humaidi

Universities attended:

Taif University, Saudi Arabia, 1999-2003
Bachelors of Science in Mathematics

University of New Brunswick, Fredericton, NB, Canada, 2011-2015
Master of Science in Applied Mathematics